Simulated Reversible Aggregation Processes for Different Interparticle Potentials: The Cluster Aging Phenomenon

G. Odriozola,[†] A. Schmitt,*[,‡] J. Callejas-Fernández,[‡] R. Martínez-García,[‡] R. Leone,[†] and R. Hidalgo-Álvarez[‡]

Departamento de Química Física y Matemática, Facultad de Química, Universidad de la República, 11800 Montevideo, Uruguay, and Departamento de Física Aplicada, Universidad de Granada, Campus de Fuentenueva, E-18071 Granada, Spain

Received: May 31, 2002; In Final Form: November 22, 2002

The kinetics of reversible 3D aggregation processes was studied for different interparticle potentials by means of simulations. In previous work (*Phys. Rev. E* **2002**, *65*, 031405),[1] freely diffusing particles were considered that aggregate whenever a collision occurs but disintegrate only with a single given breakup probability. The DLVO theory, however, predicts also interparticle potentials showing two minima of different depths separated by an energetic barrier. Hence, two different kind of bonds, primary and secondary ones, can be formed and should be treated separately. In the present work, this behavior was implemented by considering bonds with different breakup probabilities. The data obtained from simulations were compared with the stochastic solutions of the corresponding master equation. For this purpose, the Brownian kernel was employed together with novel fragmentation kernels. The agreement between the simulations and the kinetic description was found to be quite satisfactory. Moreover, studying the time evolution of the bond population showed that cluster aging appears as a natural consequence of the employed model.

1. Introduction

It is well-known that aggregation processes occur in a wide range of natural systems.[2−4] Naturally, the first studies focused on those systems that aggregate in an irreversible way.[5−8] In many cases, however, the processes show to be of a reversible nature.[9−13] In the literature, two models for irreversible aggregation processes are described. These are the diffusion-limited cluster aggregation (DLCA) and the reaction limited cluster aggregation (RLCA).[14−16] Both models assume freely diffusing clusters and, hence, approach reality only when the particles do not interact, i.e., when the interparticle potentials are of short range if compared with the particle size. The difference between both regimes lies in the stickiness of the particles. For DLCA, all cluster collisions lead to bond formation whereas for RLCA a large number of collisions is needed to produce a new cluster. These models are consistent with interparticle potentials showing a deep primary energetic minimum followed by an energetic barrier. If the interparticle potential decays fast with distance, unhindered cluster diffusion is guaranteed and a primary collision efficiency, P_1 (or primary bond formation probability), may be defined as the ratio of the number of collisions that lead to primary bond formation and the total number of collisions. Hence, P_1 increases as the energetic barrier is decreased. For $P_1 = 1$, the barrier vanishes and the DLCA regime is established.

In colloidal science, the most popular interparticle potentials are those obtained from the DLVO theory.[17−20] In many cases, this theory predicts interparticle potentials that exhibit a deep primary minimum followed by an energetic barrier, and so, the DLCA-RLCA approach excellently describes the corresponding aggregation processes. In other cases, however, the DLVO potentials present two energetic minima separated by an energetic barrier. From here on, the minimum closer to the particle surface will be called the primary minimum and the second one, further away from the particle surface, the secondary minimum. The latter is generally not deep enough to guarantee unbreakable interparticle bonds and, thus, allows for reversible aggregation. The DLCA-RLCA approach does not consider the reversible nature of these bonds and, hence, is not expected to describe all aggregation processes properly.

In ref 1, we studied the time evolution of aggregating systems where all collisions lead to the formation of bonds that are then allowed to disintegrate with a single given breakup probability. This situation models systems characterized by interparticle potentials with a finite primary minimum and no repulsive energetic barrier. Although this kind of interparticle potential is not usually found in colloidal systems, the model may be considered as a simplified approach for reversible aggregation phenomena.

In this paper, attention is focused on the study of reversible aggregation processes of more realistic systems characterized by interparticle potentials showing primary and secondary minima separated by an energetic barrier. For this purpose, the simulations are implemented in such a way that the possibility of primary and secondary minimum bond formation is taken into account. Depending on the nature of the considered primary and secondary bonds, the simulated systems are expected to evolve quite differently. Furthermore, some breakup events may be followed by immediate re-aggregation and hence, are expected to affect not only the internal cluster structure but also the nature of the corresponding bonds. The latter effect gives rise to what we call cluster aging; i.e., it allows the internal binding strength of the clusters to evolve with time.

To model the obtained cluster size distributions theoretically, the corresponding master equation is stochastically solved

[†] Universidad de la República.
[‡] Universidad de Granada.

10.1021/jp0262160 CCC: $25.00
Published on Web 02/14/2003

considering the Brownian aggregation kernel and novel fragmentation kernels. The theoretical and simulated data are then compared.

The paper is organized as follows. Section II gives the theoretical background. In section III, the simulation algorithm and the procedure for solving the master equation are described. The obtained results are shown and discussed in section IV. Here, a brief summary of the results obtained in ref 1 is also included. Finally, section V details the conclusions.

2. Theoretical Background

The master equation for reversible aggregation processes is given by[1]

$$\frac{dP(\vec{N},t)}{dt} = \frac{1}{2V}\sum_{i,j} k_{ij}[(N_i+1)(N_j+1+\delta_{ij})P(\vec{N}_{ij}^{+},t) - N_i(N_j-\delta_{ij})P(\vec{N},t)] + \frac{1}{2V}\sum_{n=2}^{\infty}[(N_n+1)\sum_{i=1}^{n-1} f_{i(n-i)}P(\vec{N}_{i(n-i)},t) - N_n\sum_{i=1}^{n-1} f_{i(n-i)}P(\vec{N},t)] \quad (1)$$

where $P(\vec{N},t)$ is the probability for finding the system in the state $\vec{N} = (N_1, N_2, ..., N_n)$ at time t, N_i is the number of i-size particles, k_{ij} is the aggregation kernel, and f_{ij} is the fragmentation kernel. The states N_{ij}^{+} and N_{ij}^{-} are given by

$$\vec{N}_{ij}^{+} = \begin{cases} (..., N_i+1, ..., N_j+1, ..., N_{i+j}-1, ...) & \text{for } i \neq j \\ (..., N_i+2, ..., N_{2i}-1, ...) & \text{for } i = j \end{cases}$$

$$\vec{N}_{ij}^{-} = \begin{cases} (..., N_i-1, ..., N_j-1, ..., N_{i+j}+1, ...) & \text{for } i \neq j \\ (..., N_i-2, ..., N_{2i}+1, ...) & \text{for } i = j \end{cases}$$

The master equation for pure aggregation and pure fragmentation processes together with a description of the algorithm employed to solve it are given in refs 21 and 22.

The aggregation kernel, k_{ij}, establishes the mean rate at which i-mers and j-mers stick and form $(i + j)$-mers. On the other hand, f_{ij} denotes the mean rate at which $(i + j)$-mers break spontaneously, generating i-mers and j-mers. Both the aggregation and the fragmentation kernels have to be understood as orientational and configurational averages of the exact aggregation rates. All physical information about the reversible aggregation mechanism is contained in the kernels.

For large clusters and long aggregation times, the solutions of the master equation can often be expressed in terms of a time-independent scaling function, $\Phi(x)$, such that

$$N_n(t) \sim s(t)^{-2}\Phi(n/s(t)) \quad (2)$$

where the argument $x = n/s(t)$ may be interpreted as a normalized cluster size.[23,24] The scaling function $s(t)$ grows asymptotically toward the weight average cluster size, $n_w = \sum_{i=1}^{\infty} i^2 N_i / \sum_{i=1}^{\infty} i N_i$.

Four different types of interparticle potentials commonly used in colloidal science are schematized in Figure 1. The arrows indicate the corresponding bond formation and breakup possibilities. Please note that the only situation that leads to pure irreversible aggregation processes corresponds to Figure 1a. Here, bond formation is achieved for very short interparticle distances once the involved particles have overcome the potential barrier. In this case, eq 1 is simplified because bond breakup cannot occur and, so, the fragmentation kernel vanishes, i.e., $f_{ij} = 0$. When no potential barrier is present, all collisions lead to bond formation and the DLCA regime is established. This regime is usually modeled by the Brownian kernel

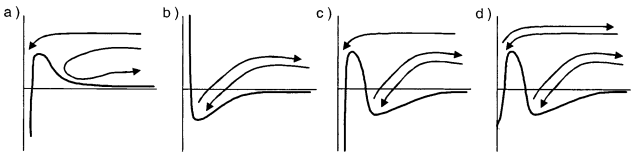

Figure 1. Schematic representation of common types of interparticle interaction potentials. (a) Infinite primary minimum with potential barrier. (b) Finite minimum. (c) Infinite primary minimum, potential barrier, and finite secondary minimum. (d) Finite primary minimum, potential barrier, and finite secondary minimum. The arrows represent the corresponding bond formation and breakup possibilities.

$$k_{ij}^{\text{Brown}} = \frac{1}{4}k_{11}^{\text{Smol}}(i^{1/d_f} + j^{1/d_f})(i^{-1/d_f} + j^{-1/d_f}) \quad (3)$$

where $k_{11}^{\text{Smol}} = 8k_BT/3\eta$ is the dimer formation rate constant, d_f is the cluster fractal dimension, k_BT is the thermal energy, and η is the solvent viscosity.[25,26] For large potential barriers, a large number of collisions is needed for aggregation and, hence, the processes become reaction controlled (RLCA). A kernel for describing such processes is given in refs 27 and 28.

Figure 1b shows an interparticle potential characterized by a finite minimum. Here, the bonds are weaker and, consequently, they have a finite average lifetime. As in the case of DLCA, all collisions lead to bond formation, and so, the aggregation kernel, k_{ij}, must be the Brownian one. For the fragmentation kernel, the following expression was deduced[1]

$$f_{ij} = e_{ij}(1 + \delta_{ij})/\tau_b \quad (4)$$

where τ_b is the characteristic decay time of an exponentially shaped bond breakup probability density function; i.e., it is the average bond lifetime. The function e_{ij} represents the average number of bonds contained in the n-sized clusters that, on breakup, lead to i- and j-size fragments. It can be obtained by averaging over all fragmentation possibilities of a vast collection of simulated cluster structures. This was done in ref 1 for loopless aggregates, yielding the following fitted expression

$$e_{ij}(1 + \delta_{ij}) = p_1(i^{p_2} + j^{p_2})(i^{p_3} + j^{p_3})(ij)^{p_4} \quad (5)$$

where $p_1 = 0.4391$, $p_2 = 1.006$, $p_3 = -1.007$, and $p_4 = -0.1363$ for the used simulation conditions.

Effective fragmentation occurs only when a bond breaks and the formed fragments diffuse away. In some cases, however, recently broken bonds may reestablish almost immediately. These cases should not be considered and so, the fragmentation kernel has to be corrected by the factor $1 - P_{Cij}$ where P_{Cij} is the probability for two recently produced fragments to collide and re-aggregate. For the simulation conditions used in ref 1, $1 - P_{Cij}$ could be approximated as $(\mathcal{N}_{11}(ij)^b)^{-1}$, where $\mathcal{N}_{11} = 6.1$ is the average number of consecutive collisions per encounter of nonaggregating monomers and $b = 0.35$ is a constant exponent.[1,27,28]

The interparticle potentials schematized in Figure 1c,d are typically predicted by the DLVO and extended DLVO theories and, thus, are of general interest for colloidal science. This article, as mentioned above, is focused on such interactions.

3. Simulations and Numerical Procedures

3.1. Simulations. The three-dimensional off-lattice simulations were performed in a square box considering periodical

boundary conditions, as explained in ref 29. The simulation parameters were established identically to those detailed in refs 1 and 27. These are a volume fraction of 5.0×10^{-4}, a step-length $l_0 = 0.5$ times the particle radius, monomeric particles at time zero, a total number of particles $N_0 = 10^4$, and a monomer diffusivity of $D_1 = 6.8 \times 10^{-13}$ m^2 s^{-1}. Additionally, the simulation procedure was slightly modified to consider the possibility of bond breakup. Because we focus on situations that correspond to interparticle potentials shown in Figure 1c,d, bonds may be formed in the primary or secondary minimum. The bonds formed in the primary minimum are characterized by a lifetime τ_{b1} that is expected to be much longer than the lifetime, τ_{b2}, of the bonds formed in the secondary minimum. To determine which kind of bond is formed when a collision takes place, a random number ξ_1 uniformly distributed in [0, 1] is generated and compared with the primary minimum bond formation probability, P_1. Evidently, P_1 gives the fraction of collisions that lead to the formation of primary bonds and $(1 - P_1) = P_2$ is the remaining fraction of collisions that give rise to the formation of secondary bonds. If the simulation time step, Δt, is small enough, i.e., $\Delta t \ll \tau_{b1}$ and $\Delta t \ll \tau_{b2}$, then $\tau_{b1} = \Delta t/P_{r1}$ and $\tau_{b2} = \Delta t/P_{r2}$, where P_{r1} and P_{r2} refer to the primary bond breakup probability and the secondary bond breakup probability, respectively. Once all clusters are moved and time is incremented a time step Δt, all bonds are checked to determine which ones might have to be broken. For that purpose, another random number, ξ_2, uniformly distributed in [0, 1], is generated for each bond and compared with P_{r1} or P_{r2}, depending on the type of the corresponding bond. When $\xi_2 < P_{r1}$ (or $\xi_2 < P_{r2}$) is verified, then the corresponding bond is broken and the fragments are separated a fixed distance $l_s = l_0/5$ in the direction of the line that connects the centers of those particles that were connected by the bond. If this new movement leads to particle overlap, the fragments are considered to re-aggregate; i.e., a new primary or secondary bond is formed following the aggregation criteria mentioned above.

3.2. Solving the Master Equation. To obtain the theoretically predicted cluster-size distributions, the master equation has to be solved using the corresponding aggregation and fragmentation kernels. For this purpose, the equivalent "stochastic simulation" approach is employed. This procedure involves the calculation of the reaction probability density function, which for pure aggregation processes may be denoted by $P(\tau,i,j)$. Here, $P(\tau,i,j)\,\mathrm{d}\tau$ is the probability that, given the state $\vec{N}$ at time t, the next reaction to take place in the volume V will be the aggregation of an i-mer with a j-mer and that this reaction will occur during the infinitesimal time interval $[t + \tau, t + \tau + \mathrm{d}\tau]$. Hence, it is convenient to define $a_{ij}\,\mathrm{d}t$ as the probability that, given the system in the state $\vec{N}$ at time t, an i-mer$-j$-mer aggregation reaction will occur inside V during $[t, t + \mathrm{d}t]$. According to ref 30, a_{ij} becomes

$$a_{ij} = \frac{N_i(N_j - \delta_{ij})k_{ij}}{V(1 + \delta_{ij})} \tag{6}$$

and the reaction probability density function

$$P(\tau,i,j) = a_{ij}\mathrm{e}^{-a_0\tau} \tag{7}$$

where $a_0 = {}^1/_2\sum_{i,j}^{N_0} a_{ij}(1 + \delta_{ij})$ and N_0 is the total number of constituting particles in the system.

The algorithm used for calculating the time evolution of the cluster size distribution is based on the above expressions. It may be summarized as follows:

1. Input: k_{ij}, initial conditions $\vec{N}(t = 0)$ and $t = 0$.
2. Calculate all a_{ij} and a_0.
3. Generate the random numbers ξ_1 and ξ_2 uniformly distributed in [0,1].
4. Increment t the amount $\tau = 1/(a_0)\ \ln(1/\xi_1)$.
5. Take the smallest pair of i and j that verifies ${}^1/_2\sum_{m,l}^{i,j} a_{ml}(1 + \delta_{ml}) > \xi_2 a_0$. Hence, the pairs of i and j cluster sizes that have a larger a_{ij} have a higher probability to be chosen.
6. Increment N_{i+j} one unit and decrement N_i and N_j one unit, too. Go back to 2 for recalculating a_{ij} and a_0. Continue with the procedure.

The procedure is finished when the system is composed by only one cluster, i.e., $a_0 = 0$. It should be noted that it is enough to recalculate a_{ij} only for those cluster sizes that have changed their population. The algorithm is explained in more detail in ref 30.

For pure fragmentation processes, the probability r_{ij} that an $(i + j)$-mer will break spontaneously into an i-mer and a j-mer inside V during $(t, t + \mathrm{d}t)$, given the system in the state $\vec{N}$ at time t, reads

$$r_{ij} = \frac{N_{i+j} f_{ij}}{V(1 + \delta_{ij})} \tag{8}$$

and so, as in the case of pure aggregation, the reaction probability density function $P(\tau,i,j)$ for pure fragmentation is given by

$$P(\tau,i,j) = r_{ij}\mathrm{e}^{-r_0\tau} \tag{9}$$

where $r_0 = {}^1/_2\sum_{i,j}^{N_0} r_{ij}(1 + \delta_{ij})$.

Therefore, the algorithm for calculating the time evolution of the cluster size distribution for reversible aggregation processes may be established as follows:

1. Input: k_{ij}, f_{ij}, $\vec{N}(t = 0)$ and $t = 0$.
2. Calculate a_{ij} and r_{ij} for all i and j. Calculate a_0 and r_0.
3. Generate the random numbers ξ_1 and ξ_2 uniformly distributed in [0,1].
4. Increment t the amount $\tau = 1/(a_0 + r_0)\ \ln(1/\xi_1)$.
5. If $a_0 \geq \xi_2(a_0 + r_0)$, take the smallest pair of i and j that verifies ${}^1/_2\sum_{m,l}^{i,j} a_{ml}(1 + \delta_{ml}) > \xi_2(a_0 + r_0)$ and continue at point 6, else continue at point 7.
6. Consider the reaction as aggregation adjusting the population of N_{i+j}, N_i, and N_j accordingly. Continue at point 2 for recalculating a_{ij} and r_{ij}, and continue with the procedure.
7. Take the first pair of i and j that verifies ${}^1/_2\sum_{m,l}^{i,j} r_{ml}(1 + \delta_{ml}) > \xi_2(a_0 + r_0) - a_0$. Here, the reaction is the breakup of an $(i + j)$-mer leading to a pair of i- and j-size fragments. Because the fragmentation may not be effective, generate another random number, ξ_3, and compare it with P_{Cij}. In case $\xi_3 < P_{Cij}$, the fragmentation is considered as not effective and so we must re-aggregate (go back to point 6). If not, continue at point 2 for recalculating a_{ij} and r_{ij}, and continue with the procedure.

Here, the system reaches an equilibrium state, and so, the procedure may be stopped when the cluster-size distribution becomes stable.

The algorithm described above considers only one kind of bonds; i.e., it works for systems characterized by interparticle potentials such as the one shown in Figure 1b. For interparticle potentials such as those shown in Figure 1c,d, the algorithm has to be slightly modified to consider the time evolution of bond populations. Figure 2 schematizes the flow diagram of the complete algorithm. Here, the number of primary bonds is denoted as E_1 and the number of secondary bonds as E_2. In the

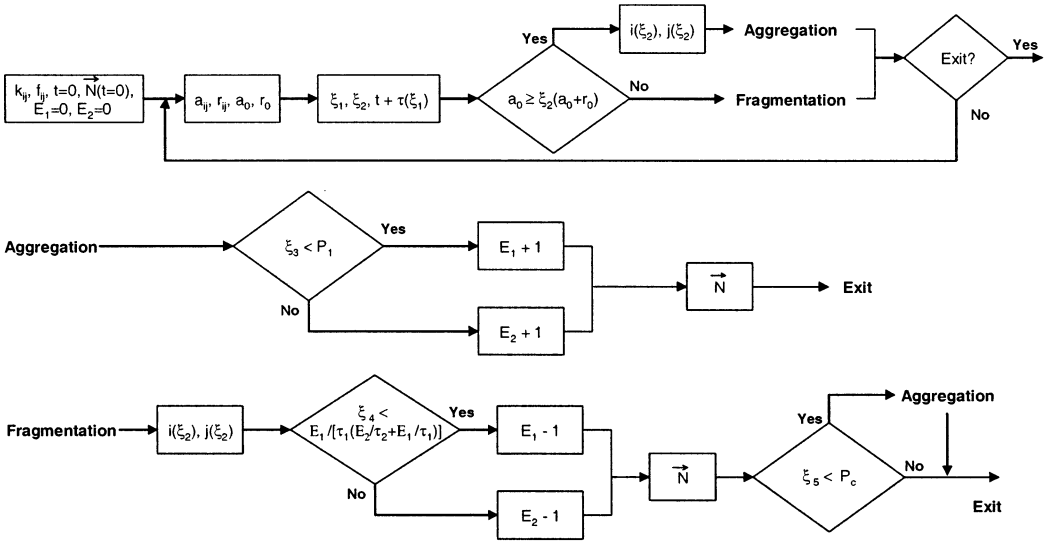

Figure 2. Flow diagram of the stochastic algorithm that considers primary and secondary bond formation.

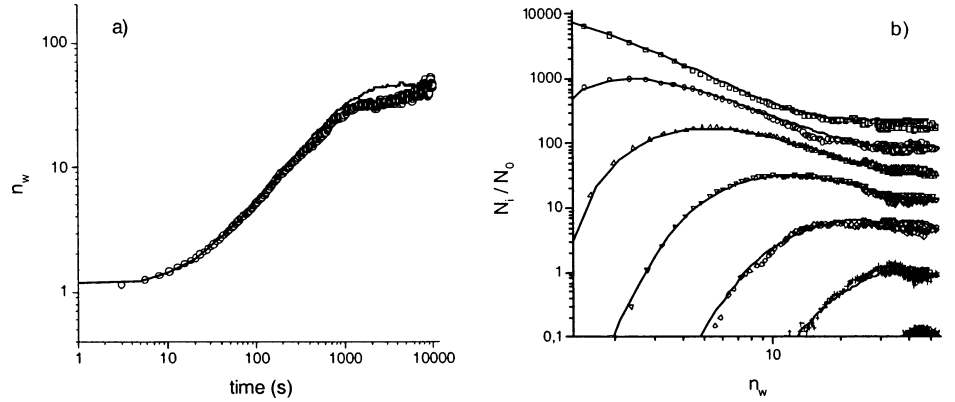

Figure 3. (a) Time evolution of the weight average cluster size, n_w, for $P_1 = 0$ and $\tau_{b2} = 196.6$ s. (b) The corresponding cluster size distribution grouped in logarithmically spaced intervals ((□) monomers, (○) 2- and 3-mers, (△) 4−8-mers, (▽) 9−18-mers, (◇) 19−38-mers, (+) 39−88-mers, and (×) 89−200-mers) as a function of n_w. In both figures, the symbols correspond to the computer simulated data whereas the solids lines correspond to the stochastic solution for the kernels given by the eqs 3 and 4.

aggregation branch, an additional random number ξ_3 is compared with P_1 to determine which kind of bond will be formed. In the fragmentation branch, a further random number ξ_4 is generated for deciding what kind of bond to break. For this purpose, ξ_4 is compared with $E_1/\tau_{b1}(E_1/\tau_{b1} + E_2/\tau_{b2})$ to account for the bond population and the mean lifetime of each kind of bond. Finally, the fragmentation effectiveness is considered in the same way as in the previously described procedure. In case of re-aggregation, the aggregation procedure is employed for deciding the nature of the reformed bond.

4. Results

In this section, we present and discuss the cluster-size distributions obtained from simulations of reversible aggregation processes. The results will be compared with the stochastic solutions of the corresponding master equation. Three different cases will be considered: equally breakable bonds, unbreakable primary bonds and breakable secondary bonds, and breakable primary and breakable secondary bonds.

4.1. Equally Breakable Bonds. This situation is thoroughly studied in ref 1 and, hence, will be described here only briefly for the sake of completeness. It corresponds to the interparticle potential shown in Figure 1b, where bonds are formed in an energetic minima of finite depth. All bonds are equal in nature, and they are characterized by a unique exponentially shaped breakup probability density function, which is characterized by the decay time or average bond lifetime, τ_b.[1]

Parts a and b of Figure 3 show the time evolution of the weight average cluster size, n_w, and the cluster size distribution as a function of n_w, obtained for the simulations having $P_1 = 0$ (only secondary bonds are allowed) and $\tau_{b2} = 196.6$ s. The curves are compared with those obtained theoretically by using the stochastic algorithm for $P_1 = 0$, k_{ij} given by equation 3 with $k_{11}^{Smol} = 11.1 \times 10^{-18}$ m^3 s^{-1} and $d_f = 2.06$, and f_{ij} given by eq 4 with $\tau_{b2} = 196.6$ s. The fractal dimension, d_f, was directly obtained from the generated structures by means of the radius of gyration method described in ref 31. It is close to the value reported in ref 32, $d_f = 2.03 \pm 0.05$ for cluster rearrangement and similar to those reached by branched polymers (lattice animals).[33,34] Please note that the effectiveness correction, $1 - P_{Cij}$, for the fragmentation kernel is already included in the simulation algorithm and, hence, f_{ij} should not re-include it.

Both figures show a good agreement between the theoretical and simulated data. At long simulation times, it can clearly be seen that the weight average cluster size tends to become time independent and to fluctuate around a given mean value in the interval.[30] This indicates that the system reaches an equilibrium state. The corresponding behavior is observed for the cluster-size distribution, which is shown in Figure 3b as a function of

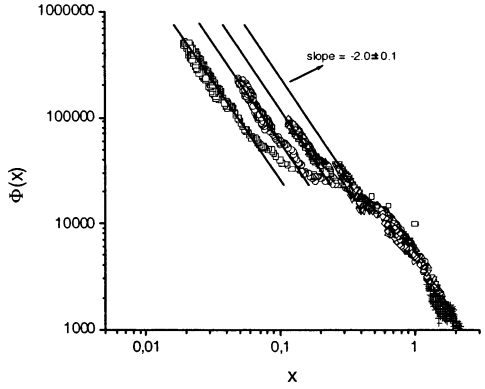

Figure 4. Dynamic scaling distribution, $\Phi(x)$, obtained for the data shown in Figure 3. The points correspond to the simulated data grouped in logarithmically spaced intervals ((□) monomers, (○) 2- and 3-mers, (△) 4−8-mers, (▽) 9−18-mers, (◇) 19−38-mers, (+) 39−88-mers, and (×) 89−200-mers).

the weight average cluster size. Also there, the number of clusters of all sizes does not change anymore, starting from average cluster sizes of about 30. Hence, all data points for large times scatter around horizontal lines in the fluctuation interval of the final average cluster size between 30 and 50. As explained in ref 1, the time spent to reach equilibrium shortens with decreasing bond lifetime, τ_{b2}. Additionally, the weight average cluster size rises to smaller values.

The corresponding scaling function $\Phi(x)$ is represented in Figure 4. It is observed that the simulated data scale only for large arguments, x. For smaller x, however, a single master curve is not established. This nonscaling region is a consequence of the fragmentation process that gains importance at longer times, i.e., for smaller arguments, x. Here, the equilibrium state also gives rise to a data accumulation at the left end of each individual curve. Note that, even though no universal scaling is observed, the different noncollapsing curves show practically the same slopes for the smaller arguments. The absolute value of these slopes were measured and averaged for the different conditions used in this study. The obtained results were 2.5 ± 0.1, 2.2 ± 0.1, 2.0 ± 0.1, 2.0 ± 0.1, and 1.8 ± 0.1 for $\tau_{b2} =$ 117.9, 147.4, 196.6, 294.8, and 598.7 s, respectively. As expected, the absolute value of the slope decreases for increasing τ_{b2} and, so, the scaling function tends toward the well-known bell-shaped DLCA curve.

4.2. Unbreakable Primary Bonds and Breakable Secondary Bonds. In this case, an interparticle potential of the type shown in Figure 1c is responsible for the bond behavior. Here, a deep energy minimum (primary) appears at short interparticle distances and a shallower secondary one at longer distances. Because no energetic barrier exists at larger distances, all collisions lead to bond formation. Nevertheless, the energetic barrier that separates both energetic minima restricts the primary bond formation. In this subsection the primary minimum is assumed to be infinite, i.e., sufficiently deep for considering the primary bonds to be unbreakable and, so, $\tau_{b1} = \infty$. As in the previous section, secondary bonds are characterized by a mean lifetime, τ_{b2}.

The simulations were carried out by setting $P_1 = 0.01$, $\tau_{b1} = \infty$, and $\tau_{b2} = 25$ s. To describe the kinetics by means of the master equation, these values were also imposed for the corresponding parameters in the aggregation and fragmentation kernels. The obtained fractal dimension, which is necessary for the Brownian kernel, was $d_f = 2.01$. Once again, this value is close to the one reported by ref 32. It indicates that cluster rearrangement processes are present. The fragmentation kernel is now given by

$$f_{ij} = \frac{e_{ij}(1 + \delta_{ij})E_2(t)}{\tau_{b2}(E_1(t) + E_2(t))} \tag{10}$$

This equation assumes that the fraction of primary and secondary bonds does not depend on the cluster size. As mentioned above, the algorithm presented in section 3 already accounts for the fragmentation effectiveness and, so, the proposed fragmentation kernel should not re-include it. It should be pointed out that cluster rearrangement occurs due to this type of noneffective breakups. In some occasions, rearrangement processes lead to primary bond formation and, hence, the clusters become less breakable. Consequently, the fragmentation rate constants diminish and the fragmentation kernel becomes time dependent. This is what we call "cluster aging". The fragmentation kernel given by eq 10 takes this effect into account through the bond population (which is time dependent).

In contrast to the previously exposed model, this aggregation mechanism concludes with a unique unbreakable N_0-size cluster. Hence, the system never reaches a dynamic equilibrium.

Figure 5a shows the time evolution of the weight average cluster size, n_w. The corresponding cluster size distribution is plotted in Figure 5b as a function of n_w. The figures also include the stochastic solutions of the master equation for the proposed aggregation and fragmentation kernels. As can be seen, a good agreement is obtained. Additionally, the bond population is shown in Figure 6a as a function of n_w. Figure 5a clearly defines three stages. The first stage occurs at the beginning of the aggregation process. Here, bond formation is much more important than bond breakup. This means that the overall process can be described by the Brownian kernel. Nevertheless, if the secondary bond lifetime is short enough, breakup processes become significant. For this stage, Figure 5a shows a substantial increase of the weight average cluster size up to approximately $n_w \simeq 8$. According to Figure 5b, an important decrease of the monomer population due to the formation of small clusters is observed in the corresponding size range of $n_w = [1, 8]$. Moreover, Figure 6a confirms that almost no primary bonds are formed during this stage and, so, practically all bonds correspond to weak aggregation in the secondary minimum.

In the second stage, the aggregation process slows down and reaches almost a pseudo-equilibrium where n_w remains close to 8 (see Figure 5a). Here, the total number of bonds and aggregates does almost not evolve with time. Nevertheless, the number of secondary bonds drastically decreases and compensates the strong increase of the primary bond population. This can clearly be seen in Figure 6a for $n_w \simeq 8$. Hence, during this stage, the secondary bonds start to break and to convert into primary bonds.

For longer times, the fraction of secondary bonds becomes almost negligible and the few secondary bonds that still remain in the system are those recently formed. In addition, the mean cluster-size increases and so does the re-aggregation probability, P_{Cij}. Therefore, the importance of the fragmentation effects drastically diminishes. This situation leads to a steep increase of n_w and, as mentioned before, the aggregation process ends when a unique unbreakable cluster is obtained. Hence, no equilibrium state is achieved and, so, the cluster-size distribution evolves always with time. Consequently, the data points do not start to scatter around horizontal lines for large cluster sizes (see Figure 5b). The curves seem to reach an asymptotic power law with an exponent of -1.07 ± 0.05. Please note that a similar asymptotic power law is also achieved by the secondary bond population.

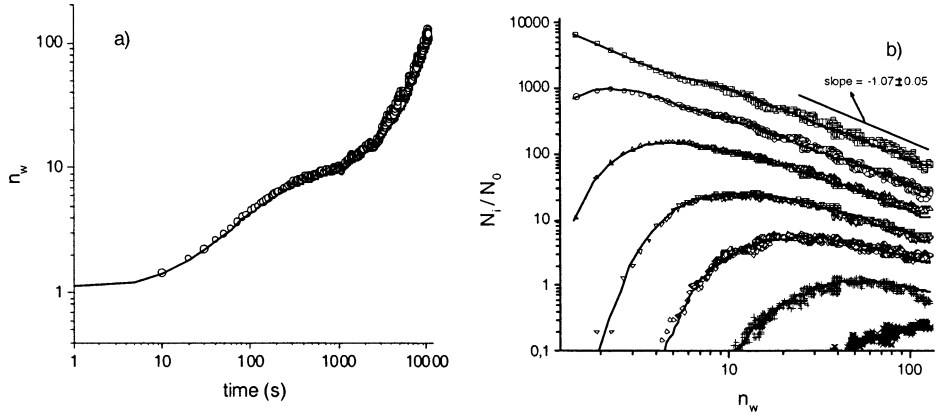

Figure 5. (a) Time evolution of the weight average cluster size, n_w, for $P_1 = 0.01$ and $\tau_{b2} = 25$ s. (b) The corresponding cluster size distribution grouped in logarithmically spaced intervals ((□) monomers, (○) 2- and 3-mers, (△) 4−8-mers, (▽) 9−18-mers, (◇) 19−38-mers, (+) 39−88-mers, and (×) 89−200-mers) as a function of n_w. In both figures, the symbols correspond to the computer simulated data whereas the solid lines correspond to the stochastic solution for the kernels given by the eqs 3 and 4.

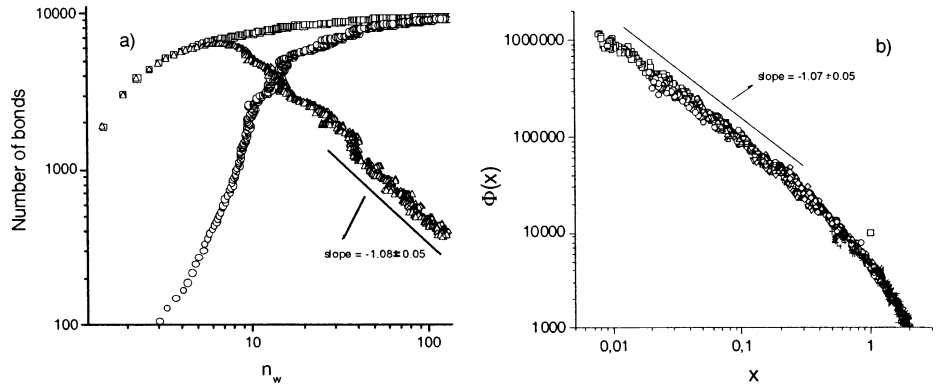

Figure 6. (a) Total number of bonds (□), number of primary bonds (○), and secondary bonds (△), for the data shown in Figure 5 as a function of n_w. (b) Dynamic scaling distribution, $\Phi(x)$, obtained from the simulated data shown in Figure 5. The data are grouped in logarithmically spaced intervals ((□) monomers, (○) 2- and 3-mers, (△) 4−8-mers, (▽) 9−18-mers, (◇) 19−38-mers, (+) 39−88-mers, and (×) 89−200-mers).

The scaling function $\Phi(x)$ obtained from the simulated data shown in Figure 5 is plotted in Figure 6b. In contrast to the previously exposed model, here, the scaling function is perfectly defined. It is surprising that the fact of including not only fragmentation but also aging effects leads to a much better defined scaling function. Furthermore, the shape of the obtained scaling function is similar to the one reported for the reaction limited cluster aggregation (RLCA) regime. The only difference lies in the initial slope, which is found to be -1.05 ± 0.05 whereas the RLCA scaling function is characterized by an initial slope of -1.5.[8,35] Considering that the cluster fractal dimension for RLCA ($d_f^{RLCA} = 2.10 \pm 0.05$) is also very close to the one obtained for this reversible regime, a detailed study of the cluster size distribution becomes very convenient as a general practice for discerning between both situations.[14−16]

4.3. Breakable Primary and Secondary Bonds. It is well-known that the DLVO theory predicts an infinitely deep energy minimum when the interparticle distance tends to zero. However, the presence of hydrated ions adsorbed onto the solid−liquid interface and hydration effects of charged surface groups limit the depth of the predicted energy minimum.[18−20] Consequently, the finite primary energetic minimum may also allow for bond breakup. In this case, one expects the relationship $\tau_{b1} \gg \tau_{b2}$ to be valid; i.e., the lifetime of primary bonds should be much larger than that of secondary bonds. As will be shown in the following paragraphs, a very small but nonzero breakup probability for primary bonds can produce significant changes in the time evolution of the systems and should basically lead to a dynamic equilibrium at sufficiently long times.

The above-mentioned case corresponds to the interparticle potential shown in Figure 1d. Essentially, it is similar in shape to the one previously studied except that it presents a noninfinite primary minimum. This allows the primary bonds to be broken, and hence, they are characterized by a finite lifetime, τ_{b1}. Consequently, the simulations need the three input parameters, P_1, τ_{b1}, and τ_{b2}. Cluster aging strongly depends on these parameters, as is true for the time evolution of the cluster size distribution. The values of $P_1 = 0.01$, $\tau_{b1} = 10000$ s, and $\tau_{b2} = 5$ s were chosen so that the main features of this type of aggregation−fragmentation processes can be shown. Evidently, these parameters were also used for solving the corresponding master equation. Furthermore, $d_f = 2.05$ was obtained by means of the radius of gyration method and used as an input parameter for the aggregation kernel. Once again, this value is close to the one reported by ref 32.

The fragmentation kernel then becomes

$$f_{ij} = e_{ij}(1 + \delta_{ij})\left[\frac{E_1}{\tau_{b1}(E_1 + E_2)} + \frac{E_2}{\tau_{b2}(E_1 + E_2)}\right] \quad (11)$$

As explained in section 4.2, the kernel should not account for the fragmentation effectiveness because it is already contained in the algorithm given in section 3. Please note that this equation considers the possibility for both, primary and secondary bond

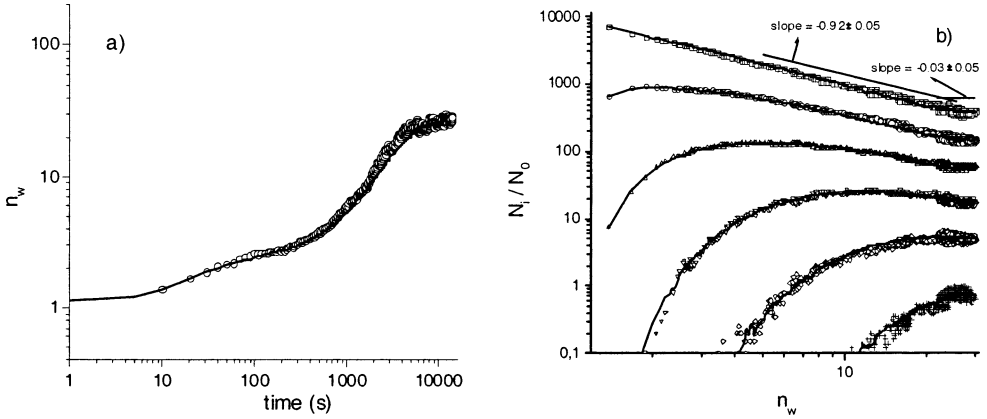

Figure 7. (a) Time evolution of the weight average cluster size, n_w, for $P_1 = 0.01$, $\tau_{b1} = 10000$ s, and $\tau_{b2} = 5$ s. (b) The corresponding cluster size distribution grouped in logarithmically spaced intervals ((□) monomers, (○) 2- and 3-mers, (△) 4−8-mers, (▽) 9−18-mers, (◇) 19−38-mers, (+) 39−88-mers, and (×) 89−200-mers) as a function of n_w. In both figures, the symbols correspond to the computer simulated data whereas the solids lines correspond to the stochastic solution for the kernels given by the eqs 3 and 4.

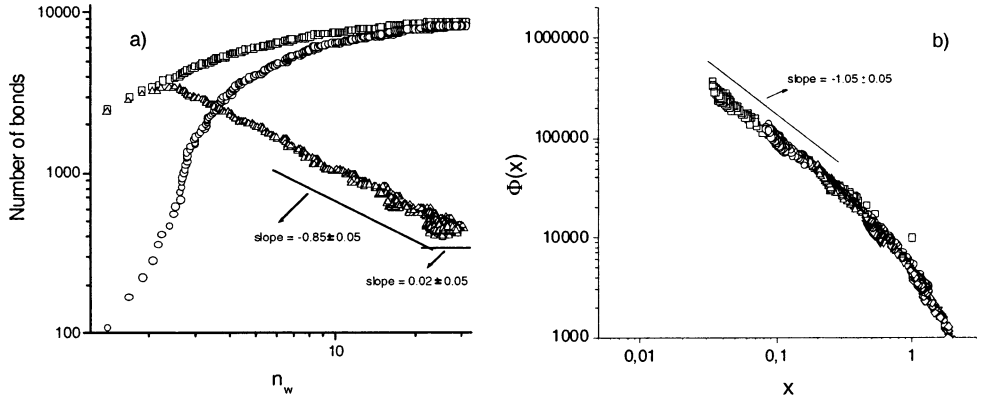

Figure 8. (a) Time evolution of the total number of bonds (□), the number of primary (○) and secondary bonds (△), for the data shown in Figure 7a. (b) Dynamic scaling distribution, $\Phi(x)$, obtained from the simulated data shown in Figure 7a. The data are grouped in logarithmically spaced intervals ((□) monomers, (○) 2- and 3-mers, (△) 4−8-mers, (▽) 9−18-mers, (◇) 19−38-mers, (+) 39−88-mers, and (×) 89−200-mers).

breakup. Equation 10, however, considers only the secondary bonds as breakable. As required, eq 11 transforms into eq 10 for $\tau_{b1} \rightarrow \infty$.

Parts a and b of Figure 7 show, just like Figure 5a,b, the time evolution of the weight average cluster size, n_w, and the cluster size distribution as a function of n_w including the simulated and theoretical data. Once again, a very good agreement is achieved.

Now, four stages may be distinguished in Figure 7a. The first three stages are very similar to those described in the previous section. Nevertheless, some minor differences should be mentioned. Due to the shorter lifetime of the secondary bonds, τ_{b2}, their population peaks at shorter times, reaching smaller values. This can be seen in Figure 8a, where, as in Figure 6a, the bond populations are plotted as a function of the average cluster size n_w. Consequently, the first stage develops with a smaller overall aggregation velocity and, so, the weight average cluster size, n_w, reaches smaller values ($n_w \simeq 3$). Furthermore, the duration of this stage is shorter. In fact, the second and third stages also shortened due to the same reason. This slower overall aggregation rate can also be noted by comparing Figures 7b and 5b where the distance between two consecutive curves is much larger and only a few 39- to 88-mers appear. It should be also noted that the curves reach the dynamic equilibrium with a significantly smaller slope than the ones of Figure 5b. Evidently, the dynamic equilibrium is characterized by a slope close to zero.

The effect of considering the possibility of primary bond breakup mainly appears at long times. The third stage, where the number of secondary bonds is not important when compared with the number of primary ones, starts suffering primary bond breakup and, so, gives rise to a decreasing overall aggregation velocity. Here, a single primary bond breakup event leads to consecutive formations and breakups of many secondary bonds until a new primary bond is reobtained. This leads to a slower decrease of the secondary bond population, which can be seen by comparing Figures 6a and 8a. This is why a very large but finite primary bond lifetime considerably affects the time evolution of the bond population and the cluster size distribution.

During the final fourth stage, the cluster size distribution and bond population reach a dynamic equilibrium and fluctuate around the corresponding mean values. Hence, the curves shown in Figures 7b and 8a stop once the equilibrium state is established and the data points for large times scatter around horizontal lines in the fluctuation interval of the final average cluster size $n_w = [22, 30]$.

As expected, the equilibrium cluster-size distribution and bond populations depend on P_1, τ_{b1}, and τ_{b2}. For example, a decreasing τ_{b2} leads to a smaller weight average cluster size and shortens the third stage. An increasing τ_{b1} gives rise to a longer first stage and to an increase in the weight average cluster size during the second and fourth stages. If P_1 is decreased, the equilibrium stage is reached at longer times and for larger cluster sizes.

The scaling function, $\Phi(x)$, corresponding to the cluster-size distribution shown in Figure 7b, is drawn in Figure 8b. Also here, a well-defined scaling behavior is observed. Please note that it does not differ very much from the one obtained for the

irreversible primary bond model. In fact, the measured slope for small x was -1.07 ± 0.05, which is practically the same as the slope obtained from Figure 6b. Here, however, the scaling function ends for small x and all remaining data points for large times scatter around that point. This means that the only effect of a small but finite primary break-up probability on $\Phi(x)$ seems to be a truncation of the scaling function at small x.

It should be pointed out that the mentioned internal cluster rearrangement processes due to noneffective bond breakup are not equal in nature with the one occurring in real systems. Real cluster rearrangement takes place even when the bonds are not broken and reestablished. It just exists as a consequence of internal relative displacements between weakly bound particles.[36−41] Depending on its extent, this phenomenon may lead to more compact clusters characterized by a higher fractal dimension. Furthermore, it is also expected to affect the fragmentation scheme because looplike structures become favored and, so, the breakup of a given bond would not necessarily lead to two separated clusters. Hence, real aggregates with the same bond strengths are expected to show a lower fragmentation activity than the one considered by our model. Indeed, eq 5 is strictly valid only for dimer fragmentation whereas the discrepancies with looplike structures should increase with cluster size. In summary, care should be taken if one tries to compare the predictions of the presented model with experimental data obtained for systems where weak bonds and looplike structures are expected. Nevertheless, the observed differences may even help to study the importance of internal restructuring processes, which are not due to the breakup and reestablishing of weak bonds.

5. Conclusions

As a first step, only reversible aggregation into the secondary minimum was studied assuming that all formed bonds are of identical nature in the sense that they are characterized by the same exponentially shaped breakup probability density function. As expected, the model predicts an equilibrium state at sufficiently long times, which depends on the average bond lifetime. Here, the scaling function $\Phi(x)$ is well defined only for larger arguments, x. Furthermore, cluster rearrangement processes appear. Nevertheless, no cluster aging is observed; i.e., the fragmentation kernel is not time dependent.

As a second step, two different kinds of bonds are allowed to be formed, primary and secondary ones. Each type is characterized by different average lifetimes, τ_{b1} and τ_{b2}. These models are consistent with the interparticle potentials obtained from the DLVO theory. In this case, cluster rearrangement processes also give rise to cluster aging due to the fact that secondary bonds may, on breakup, transform into primary ones. Here, a well-defined dynamic scaling function, $\Phi(x)$, is obtained.

Depending on the nature of the primary bonds, unbreakable or not, the cluster size distribution behaves in quite different ways. This change is important even when the average primary bond lifetime is much larger than the one of the secondary bonds. For unbreakable primary bonds, the aggregation process ends when a unique unbreakable N_0-size cluster is formed. On the contrary, a dynamic equilibrium state is achieved for the breakable primary bond model.

It should also be pointed out that all simulated data were in complete agreement with those obtained by solving the stochastic master equation, and hence, we may conclude that the proposed aggregation and fragmentation kernels describe the kinetics of the studied reversible aggregation processes quite properly.

Acknowledgment. The financial support from the Ministerio de Ciencia y Tecnologia, Plan Nacional de Investigacion, Desarrollo e Innovacion Tecnologica (I + D + I), project MAT 2000-1550-C03-01 is also acknowledged. G.O. is grateful for financial support granted by the CSIC (Exp. 004010-001187-01) and PEDECIBA (Uruguayan organization).

References and Notes

(1) Odriozola, G.; Schmitt, A.; Moncho-Jordá; Callejas-Fernández, J.; Martínez-García, R.; Leone, R.; Hidalgo-Álvarez, R. Constant bond breakup probability model for reversible aggregation processes. *Phys. Rev. E* **2002**, *65*, 031405.

(2) Family, F.; Landau, D. P. *Kinetics of Aggregation and Gelation*; North-Holland: Amsterdam, 1984.

(3) Sonntag, H.; Strenge, K. *Coagulation Kinetics and Structure Formation*; Plenum Press: New York, 1987.

(4) Meakin, P. *Fractals, scaling and growth far from equilibrium*; Springer: Cambridge, U.K., 1998.

(5) Weitz, D. A.; Oliveria, M. Fractal structures formed by kinetic aggregation of aqueous gold colloids. *Phys. Rev. Lett.* **1984**, *52*, 1433.

(6) Meakin, P. Formation of fractal clusters and networks by irreversible diffusion-limited aggregation. *Phys. Rev. Lett.* **1983**, *51*, 1119.

(7) Ernst, M. H. Kinetics of clustering in irreversible aggregation. In *Fractals in Physics*; Pietronero, L., Ed.; North-Holland: Amsterdam, 1986.

(8) Broide, M. L.; Cohen, R. J. Experimental evidence of dynamic scaling in colloidal aggregation. *Phys. Rev. Lett.* **1990**, *64* (17), 2026−2029.

(9) Family, F.; Meakin, P.; Deutch, J. M. Kinetics of coagulation with fragmentation: Scaling behavior and fluctuations. *Phys. Rev. Lett.* **1986**, *57* (6), 727−730.

(10) Meakin, P.; Ernst, M. H. Scaling in aggregation with breakup simulations and mean-field theory. *Phys. Rev. Lett.* **1988**, *60* (24), 2503−2506.

(11) Pefferkorn, E.; Stoll, S. Aggregation/fragmentation processes in unstable latex suspension. *J. Colloid Interface Sci.* **1990**, *138* (1), 261−272.

(12) Pefferkorn, E.; Widmaier, J. Aggregation and fragmentation processes of lyophobic and hydrated colloids. *Colloids Surf.* **1998**, *145*, 25−35.

(13) Elfarissi, F.; Pefferkorn, E. Fragmentation of kaolinite aggregates induced by ion-exchange reactions within adsorbed humic acid layers. *J. Colloid Interface Sci.* **2000**, *221*, 64−74.

(14) Lin, M. Y.; Lindsay, H. M.; Weitz, D. A.; Klein, R.; Ball, R. C.; Meakin, P. Universal diffusion-limited colloid aggregation. *Phys. Condens. Matter* **1990**, *2*, 3093−3113.

(15) Lin, M. Y.; Lindsay, H. M.; Weitz, D. A.; Ball, R. C.; Klein, R.; Meakin, P. Universal reaction-limited colloid aggregation. *Phys. Rev. A* **1990**, *41* (4), 2005−2020.

(16) Odriozola, G.; Tirado-Miranda, M.; Schmitt, A.; Martínez-López, F.; Callejas-Fernández, J.; Martínez-García, R.; Hidalgo-Álvarez, R. A light scattering study of the transition region between diffusion- and reaction-limited cluster aggregation. *J. Colloid Interface Sci.* **2001**, *240* (1), 90−96.

(17) Verwey, E. J. W.; Overbeek, J. T. G. *Theory of the Stability of Lyophobic Colloids*; Elsevier Publishing Co., Inc.: Amsterdam, 1948.

(18) Hunter, R. J. *Foundations of Colloid Science*; Clarendon Press: Oxford, U.K., 1987.

(19) Israelachvili, J. N. *Intermolecular and Surface Forces*, 2nd ed.; Academic Press: New York, 1991.

(20) Evans, F.; Wennerström, H. *The Colloidal Domain*, 2nd ed.; Wiley-VCH: New York, 1999.

(21) Thorn, M.; Seesselberg, M. Dynamic scaling in colloidal aggregation: Comparison of experimental data with results of a stochastic simulation. *Phys. Rev. Lett.* **1994**, *72* (22), 3622.

(22) Thorn, M.; Broide, M. L.; Seesselberg, M. Fluctuations in discrete fragmentation processes studied by stochastic simulations. *Phys. Rev. E* **1995**, *51* (5), 4089−4094.

(23) van Dongen, P. G. J.; Ernst, M. H. Dynamic scaling in the kinetics of clustering. *Phys. Rev. Lett.* **1985**, *54* (13), 1396−1399.

(24) van Dongen, P. G. J.; Ernst, M. H. Scaling solutions of smoluchowski's coagulation equation. *J. Statist. Phys.* **1988**, *50* (1/2), 295−329.

(25) von Smoluchowski, M. Versuch einer mathematischen theorie der koagulationskinetik kolloider lösungen. *Z. Phys. Chem.* **1917**, *92*, 129−168.

(26) von Smoluchowski, M. Drei vorträge über diffusion, brownsche molekularbewegung und koagulation von kolloidteilchen. *Phys. Z.* **1916**, *17*, 557.

(27) Odriozola, G.; Moncho-Jordá, A.; Schmitt, A.; Callejas-Fernández, J.; Martínez-García, R.; Hidalgo-Álvarez, R. A probabilistic aggregation

kernel for the computer-simulated transition from dlca to rlca. *Europhys. Lett.* **2001**, *53* (6), 797−803.

(28) Moncho-Jordá, A.; Odriozola, G.; Martínez-López, F.; Schmitt, A.; Hidalgo-Álvarez, R. The DLCA-RLCA transition arising in 2D-aggregation: simulations and mean field theory. *Eur. Phys. J. E* **2001**, *5*, 471−480.

(29) Schmitt, A.; Odriozola, G.; Moncho-Jordá, A.; Callejas-Fernández, J.; Martínez-García, R.; Hidalgo-Álvarez, R. Multiple contact kernel for diffusionlike aggregation. *Phys. Rev. E* **2000**, *62* (6), 8335−8343.

(30) Gillespie, D. T. Exact stochastic simulation of coupled chemical reactions. *J. Phys. Chem.* **1977**, *81* (25), 2340−2361.

(31) Vicsek, T. *Fractal Growth Phenomena*, 2nd ed.; World Scientific: Singapore, 1992.

(32) Kolb, M. Reversible diffusion-limited cluster aggregation. *J. Phys. A: Math. Gen.* **1986**, *19*, L263−L268.

(33) Wessel, R.; Ball, R. C. Diffusion-limited aggregation at equilibrium. *Phys. Rev. A* **1992**, *45* (4), R2177−R2178.

(34) Wessel, R.; Ball, R. C. Fractal aggregates and gels in shear flow. *Phys. Rev. A* **1992**, *46* (6), R3008−R3011.

(35) Broide, M. L.; Cohen, R. J. Measurements of cluster-size distributions arising in salt-induced aggregation of polystyrene microspheres. *J. Colloid Interface Sci.* **1992**, *153* (2), 493−508.

(36) Tirado-Miranda, M.; Schmitt, A.; Callejas-Fernández, J.; Fernández-Barbero, A. Experimental evidence of rearrangement in fractal clusters. *Prog. Colloid Polym. Sci.* **1998**, *110*, 110−113.

(37) Tandon, P.; Rosner, D. E. Monte carlo simulation of particle aggregation and simultaneous restructuring. *J. Colloid Interface Sci.* **1999**, *213* (2), 273−286.

(38) Tirado-Miranda, M.; Schmitt, A.; Callejas-Fernández, J.; Fernández-Barbero, A. Colloidal clusters with finite binding energies: Fractal structure and growth mechanism. *Langmuir* **1999**, *15*, 3437−3444.

(39) Cipelletti, L.; Manley, S.; Ball, R. C.; Weitz, D. A. Universal aging features in the restructuring of fractal colloidal gels. *Phys. Rev. Lett.* **2000**, *84* (10), 2275−2278.

(40) Fernandez-Nieves, A.; van Duijneveldt, J. S.; Fernandez-Barbero, A.; Vincent, B.; de las Nieves, F. J. Structure formation from mesoscopic soft particles. *Phys. Rev. E* **2001**, *64* (5), 051603.

(41) Mellema, M.; Walstra, P.; van Opheusden, J. H. J.; van Vliet, T. Effects of structural rearrangements on the rheology of rennet-induced casein particle gels. *Adv. Colloid Interface Sci.* **2002**, *98* (1), 25−50.